Earth Syst. Dynam., 17, 1765–1778, 2026
https://doi.org/10.5194/esd-17-1765-2026
© Author(s) 2026. This work is distributed under
the Creative Commons Attribution 4.0 License.

Earth System Dynamics
Open Access
EGU

Research article

Present and future responses of near-surface wind speed to different land-use and land-cover types in China

Hui-Shuang Yuan[1], **Yang Xu**[1], **Zhi-Da Sun**[1], **Zi-Han Wang**[1], **Youli Chang**[1], **and Cheng Shen**[2]

[1]Department of Atmospheric Science, Yunnan University, Kunming, China
[2]Department of Earth Sciences, University of Gothenburg, Gothenburg, Sweden

Correspondence: Youli Chang (ylchang@ynu.edu.cn) and Cheng Shen (cheng.shen@gu.se)

Received: 6 April 2026 – Discussion started: 27 April 2026
Revised: 29 September 2026 – Accepted: 30 September 2026 – Published: 23 November 2026

Abstract. Near-surface wind speed (NSWS) is highly sensitive to land-use and land-cover change (LULCC). However, previous studies have mainly focused on overall LULCC effects, leaving the attribution of wind variations to individual land transitions and management poorly constrained. Here, we utilize simulations from the latest Land-Use Model Intercomparison Project to disentangle and quantify the responses of NSWS to different types of LULCC over China from 1970 to 2014. We demonstrate that the primary-to-grazing transition is the dominant factor contributing to LULCC-induced NSWS variability, followed by fertilizer use, while urbanization makes the smallest contribution among the examined LULCC types. Future projections further suggest that land-use pathways can substantially perturb wind patterns, with low-emission pathways combined with minimally regulated land use producing more pronounced alterations than high-emission pathways combined with sustainable land use. These results highlight the importance of resolving LULCC in attributing and projecting NSWS changes, with implications for climate modeling, wind-energy assessment, and land-use policy.

1 Introduction

10-m near-surface wind speed (NSWS) is a critical variable influencing atmospheric processes and environmental systems (Zha et al., 2016). NSWS is vital for understanding climate variability as it affects the evaporation of surface water and thus influences the water cycle (Minola et al., 2024; Dunn et al., 2022). Furthermore, NSWS is essential for supporting renewable energy development, acting as the direct source of wind power needed to mitigate climate change (Pryor and Barthelmie, 2021; Zha et al., 2021c; Shen et al., 2024; Dunn et al., 2022; Shen et al., 2023). A widespread decline in NSWS, referred to as "stilling", was observed across more than 70 % of mid-latitude land stations in the Northern Hemisphere between the 1980s and 2010s (Vautard et al., 2010; Yan et al., 2026; Minola et al., 2023). A similar decline has also been observed in China, with the largest NSWS reduction occurring in spring and the largest increase during the recent recovery occurring in autumn, raising concerns about the future evolution and underlying causes of NSWS changes (Zha et al., 2021b; Yang et al., 2021; Xu et al., 2026). In contrast to this decline over land, marine NSWS increased before 2010 (Zheng et al., 2016), and this land–ocean contrast highlights the key role of land-surface modifications in terrestrial stilling. Reanalysis datasets, which are considered to have limited sensitivity to land-use and land-cover change (LULCC) effects, generally fail to replicate this observed slowdown, suggesting the need to better incorporate surface roughness into weather and climate models (Vautard et al., 2010; Zeng et al., 2019; Shen et al., 2026).

Previous attribution studies of NSWS changes related to LULCC have largely relied on a limited number of land-use processes, which may have hindered a deeper understanding of the role of LULCC. For instance, existing studies have largely linked these NSWS changes to urbanization, based on comparisons between urban and rural meteorological measurements (Wang et al., 2020; Li et al., 2018). However, inconsistencies in the definitions of urban and rural, alongside variations in methodological approaches, have introduced significant uncertainties (Li et al., 2008). Using high-resolution aerodynamic roughness length data, recent studies

estimate that urbanization accounts for approximately 11 % of the observed NSWS reductions in China, with the most significant impacts occurring in southeastern China (Zhang et al., 2019). Although such studies support the importance of surface roughness changes for NSWS, it remains challenging to determine whether these modifications are strictly driven by urbanization. Other concurrent LULCC processes, including the transition of natural land to managed pastures and widespread fertilizer application, modify not only surface friction but also boundary-layer stability, implying that the non-urban drivers of NSWS variations might be vastly underestimated (Wu et al., 2025; Zhang et al., 2025; Tran et al., 2017; Christidis et al., 2013; Sierra et al., 2022).

Despite this complexity, quantitative assessments of individual LULCC types focus predominantly on urbanization, and analyses of other processes, such as land-state transitions and land-management practices, remain scarce (Liu et al., 2024; Shen et al., 2021; Chuan et al., 2024; Andres-Martin et al., 2023; Shen et al., 2026). In addition, different vegetation and land-cover types can influence NSWS through multiple complex pathways. Previous studies have focused on aerodynamic roughness, whereas other physical pathways, such as local temperature changes and near-surface circulation variations driven by surface albedo, have received much less attention (Wang et al., 2025, 2024; Zha et al., 2021a). As a result, the specific responses of NSWS to distinct types of land-cover change remain poorly constrained. Moreover, the future implications of LULCC under different emission scenarios have also received limited attention, leaving substantial gaps in our understanding of projected NSWS changes.

To address these gaps, we combine experiments from the Land-Use Model Intercomparison Project (LUMIP) of the Coupled Model Intercomparison Project Phase 6 (CMIP6) with ridge regression to investigate the effects of LULCC on NSWS over China. Specifically, we quantify the contributions of individual LULCC types, including land-use transitions and management practices, during 1970–2014 and assess the impacts of future LULCC on NSWS. The remainder of this paper is structured as follows: Sect. 2 details the data sources and methods. Section 3 presents the results. Section 4 summarizes the main conclusions and discusses the implications for climate modeling, renewable energy planning, and land management.

2 Materials and methods

2.1 Global climate models

To quantify the impact of LULCC on NSWS, we employed simulations from the LUMIP, part of the CMIP6 (O'Neill et al., 2016). The LUMIP is an endorsed CMIP6 activity that provides targeted experiments to quantify the impacts of land states and management on climate (Lawrence et al., 2016). In CMIP6, the standard historical experiment includes all anthropogenic and natural forcings, with prescribed LULCC. LUMIP adds a complementary experiment, hist-noLu, in which land-use and management are fixed at 1850 levels. Comparing the CMIP6 historical experiments with the LUMIP hist-noLu helps isolate the contribution of LULCC to NSWS (Santos et al., 2023).

For future projections, we analyzed two Shared Socioeconomic Pathways (SSPs): SSP1-2.6 and SSP3-7.0. SSP1-2.6 represents a low-emission pathway with sustainable land-use management, and SSP3-7.0 depicts a high-emission pathway with extensive land-use expansion (Ito and Hajima, 2020). Specifically, SSP1-2.6 emphasizes sustainable land management with extensive reforestation and constrained agricultural expansion, whereas SSP3-7.0 assumes minimal environmental regulation, leading to substantial cropland and pasture expansion at the expense of forests (Popp et al., 2017). Additional sensitivity experiments ("ssp126-ssp370Lu" and "ssp370-ssp126Lu") swapped land-use datasets between the two scenarios to isolate the effects of varying land-use intensities under contrasting emission pathways (Tang et al., 2023). Comparing these experiments with their parent scenarios (SSP1-2.6 and SSP3-7.0, respectively) quantifies how NSWS would change in future scenarios in which only land-use policy is altered, which can indicate the potential impacts of LULCC in future. Details of these scenarios are presented in Table 1. All model outputs were bilinearly interpolated onto a $1^\circ \times 1^\circ$ grid, and annual means were used. Details of the model experiments used are provided in Table 2.

2.2 Gridded observational data

The monthly CN05.1 dataset (Wu and Gao, 2013), providing a spatial resolution of $0.25^\circ \times 0.25^\circ$, serves as a reliable reference for assessing observed NSWS variations and benchmarking model simulations (Chuan et al., 2024; Shen et al., 2022b; Li et al., 2024; Li et al., 2025; Zha et al., 2024). In this study, CN05.1 was interpolated to a $1^\circ \times 1^\circ$ grid and used to evaluate the performance of the global climate models in simulating NSWS changes over China from 1970 to 2014 (Wu et al., 2017; Long et al., 2021). CN05.1 also served as the dependent variable of the ridge regression and as the reference for assessing how well the ridge-regression calibration corrects the models (Sect. 2.5).

2.3 Land-use harmonization dataset

We employed the Land-Use Harmonization 2 (LUH2) dataset, a global gridded dataset designed for climate modeling, to analyze the NSWS response to LULCC roles (Hurtt et al., 2020). The LUH2 dataset provides annual data at $0.25^\circ \times 0.25^\circ$ resolution, incorporating updated inputs and detailed representations of land-use states, transitions and agricultural management (Chini et al., 2021; Hurtt et al., 2020). For this study, LUH2 data during 1970–2014 were selected. To ensure compatibility with other datasets and mod-

Table 1. List of experiments from CMIP6 used in this study.

Experiment name	Experiment Forcings	Description
historical	Historical with all forcings	CMIP6 historical simulation
hist-noLu	Historical with fixed LULCC forcings	CMIP6 historical simulation with land use kept constant at 1850 pre-industrial level
ssp126	Projection with SSP1-2.6 scenario	CMIP6 low forcing scenario projection based on SSP1-2.6
ssp126-ssp370Lu	SSP1-2.6 with SSP3-7.0 land use	Same as SSP1-2.6 except for use of SSP3-7.0 land use scenario
ssp370	Projection with SSP3-7.0 scenario	CMIP6 high forcing scenario projection based on SSP3-7.0
ssp370-ssp126Lu	SSP3-7.0 with SSP1-2.6 land use	Same as SSP3-7.0 except for use of SSP1-2.6 land use scenario

Table 2. Global climate models selected from CMIP6.

Model name	Number of ensemble members	Institution	Resolution (lat × lon)
ACCESS-ESM1-5	10	Commonwealth Scientific and Industrial Research Organisation, Australia	145 × 192
BCC-CSM2-MR	1	Beijing Climate Center, China	160 × 320
CanESM5	10	Canadian Centre for Climate Modelling and Analysis, Canada	64 × 128
CMCC-ESM2	1	Fondazione Centro Euro-Mediterraneo sui Cambiamenti Climatici, Italy	192 × 288
IPSL-CM6A-LR	4	Institut Pierre Simon Laplace, France	143 × 144
MIROC-ES2L	1	Japan Agency for Marine-Earth Science and Technology, Japan	64 × 128
MPI-ESM1-2-LR	1	Max Planck Institute for Meteorology, Germany	96 × 192
NorESM2-LM	1	NorESM Climate modeling Consortium, Norway	96 × 144
UKESM1-0-LL	4	Met Office Hadley Centre, UK	144 × 192

els, all fields were interpolated to a $1^\circ \times 1^\circ$ grid. The dataset provides three LULCC types: states, transitions, and management. In LUH2, land cover is divided into 12 LULCC types (Hurtt et al., 2020). For each grid cell, land-use states are provided as area fractions and transitions as annual conversion areas, allowing multiple land-use types to coexist within the same grid cell. To obtain more interpretable results and to avoid overparameterization in the ridge regression, we merge these into five broad categories. The merging scheme is informed by Hurtt et al. (2020), with the specific mapping detailed in Table 3.

The state and management variables represent, for each year, the land-use composition and management intensity in each grid cell. In contrast, transition records year-to-year variations between land-use types, i.e., the change from one year to the next (records labeled with a given year refer to the change between that year and the following year). To pair land-use change with NSWS for a given year, we sum transitions through the previous year so that the cumulative land-use change history aligns with the state, management, and LULCC-induced NSWS for that year.

2.4 Impact of LULCC on NSWS

The historical and hist-noLu experiments from LUMIP provide a controlled framework to isolate the contribution of

Table 3. Management categories and LUH2 state-type aggregation scheme.

State	
Cropland	C3 annual crops (c3ann); C3 nitrogen-fixing crops (c3nfx); C3 perennial crops (c3per); C4 annual crops (c4ann); C4 perennial crops (c4per)
Grazing	Managed pasture (pastr); rangeland (range)
Primary	Forested primary land (primf); non-forested primary land (primn)
Secondary	Potentially forested secondary land (secdf); potentially non-forested secondary land (secdn)
Urban	Urban land
Management	
Fertl	Fertilization
Irrig	Irrigation

LULCC to NSWS, which is difficult to disentangle using observations alone. The historical simulations incorporated observed LULCC, including land-use transitions and management practices, whereas land use in "hist-noLu" is fixed at its 1850 level. Therefore, the change of NSWS caused by LULCC could be calculated as:

$$\mathrm{NSWS}_{\text{LULCC-induced}} = \mathrm{NSWS}_{\text{historical}} - \mathrm{NSWS}_{\text{hist-nolu}}, \quad (1)$$

For future, we analyze the LUMIP experiments ssp126-ssp370Lu and ssp370-ssp126Lu, which replace each scenario's LULCC forcing with that from the other scenario. The former retains all forcings other than land use from SSP1-2.6 while applying the SSP3-7.0 land-use forcing (LUH2 states, transitions, management, and harvest), whereas the latter retains the SSP3-7.0 background while applying the SSP1-2.6 land-use forcing. Comparing each swap experiment with its parent scenario (e.g., ssp126-ssp370Lu versus ssp126) provides an estimate of the LULCC contribution to NSWS under low- and high-emissions backgrounds, thereby probing interactions between emissions and land use. From a policy perspective, ssp126-ssp370Lu can be broadly interpreted as a low-emission pathway with less stringent land-use management, whereas ssp370-ssp126Lu represents a high-emission pathway with more sustainable land-use management. More specifically, the difference between ssp126-ssp370Lu and ssp126 quantifies the NSWS response to the contrast between these land-use management pathways under a low-emissions background, whereas the difference between ssp370 and ssp370-ssp126Lu quantifies the same contrast under a high-emissions background. Comparing these responses allows a direct assessment of how the effect of LULCC on NSWS depends on the emissions background.

2.5 Ridge regression analysis

To reduce uncertainty from model deficiencies, we applied ridge regression to calibrate model weights based on their skill in reproducing historical NSWS changes (Hoerl and Kennard, 1970). All variables were standardized to ensure comparability across units and scales beforehand. The ridge penalty shrinks large coefficients, mitigates multicollinearity, and yields a balanced integration that avoids overemphasizing any single model (Tebaldi and Knutti, 2007). The historical simulations of individual models were used as independent variables, while observational data served as the dependent variable. The regression was fitted independently at each $1^\circ \times 1^\circ$ grid cell. The relationship can be described as Eq. (2):

$$\mathrm{NSWS}_{\text{obs}} = \sum R_i M_i + \mathrm{Res}, \quad (2)$$

where $\mathrm{NSWS}_{\text{obs}}$ represents the reference, which is the CN05.1 dataset in this study. M_i denotes the standardized historical experiment series from the model. R_i is the corresponding regression coefficient. The ridge penalty parameter (α) was selected using leave-one-out cross-validation from 100 logarithmically spaced candidate values between 10^{-6} and 10^{6}. For each candidate α, one sample was withheld in turn, and the model was fitted using the remaining $n-1$ samples and evaluated by predicting the withheld sample. The α yielding the lowest mean squared prediction error across all held-out samples was selected. The model was then refitted using all available samples with the selected α to obtain the final regression coefficients.

Ridge regression was also used in the subsequent attribution analysis. During model calibration, to ensure the ridge regression-based information is a valid rather than artificial signal (i.e., to avoid negative correlations between observations and model predictors), all R_i are constrained to be non-negative.

2.6 Contributions of various LULCC types

We apply ridge regression to quantify the contributions of land states and transitions on NSWS, leaving coefficient signs unconstrained since negative associations can be reasonable. As in Sect. 2.5, the regressions in this section are fitted independently at each grid cell. Different land use

types and transitions describe related aspects of land surface change and may therefore introduce multicollinearity, which can destabilize conventional regression estimates and hinder the attribution of individual contributions. Ridge regression was used to address this issue by applying a penalty term that shrinks the coefficients of correlated predictors and stabilizes their estimates. All variables were standardized to the same scale before model fitting, so that predictors with small magnitudes, such as those related to urban land use, were not assigned disproportionately small coefficients. The effects of different LULCC types on NSWS were quantified in two steps. Specifically, we posit that the LULCC-driven component of NSWS depends on land states and management. Different land states and management practices in LUH2 may be associated with different expected wind speeds. Accordingly, we approximate this dependence with ridge regression that links land states and management indicators to the LULCC-induced NSWS following Eq. (3):

$$\mathrm{NSWS}_{\mathrm{LULCC\text{-}induced}} = \sum\nolimits_{k\in S} R_k X_k + \mathrm{Res}, \tag{3}$$

Here, the index set S includes five land states (cropland, grazing, primary, secondary, urban) and two management practices (fertilization and irrigation). X represents the area of each land state, the irrigated area, or the total nitrogen fertilizer rate across all crop types, during 1970–2014. The relative contribution of each explanatory variable to LULCC-induced variability was calculated following Eq. (4):

$$\mathrm{RC}_i = \frac{|R_i|}{\sum_i |R_i|}, \tag{4}$$

where $|R_i|$ is the absolute value of the regression coefficient of its explanatory variable. This approach, grounded in regression coefficient analysis, allows for clearer interpretation of the proportional impact of each variable within the model (Bring, 1994; Grömping, 2006).

For each land state, we interpret the corresponding linear term in Eq. (3) as a proxy for the portion of LULCC-induced NSWS associated with that state. This state-level contribution is then further attributed to specific transition types and, where applicable, harvest (in LUH2, harvest denotes wood harvest from primary and secondary land; Hurtt et al., 2020). Therefore, we employ the ridge regression again to link the contribution of specific land states and relevant transitions and harvest following Eq. (5):

$$R_{\text{state A}} X_{\text{state A}} = \sum\nolimits_{i\in S(\text{state A})} R_i Y_i + \mathrm{Res}, \tag{5}$$

The relative contribution of a given term is computed as:

$$\mathrm{RC}_{\text{state A to state B}} = \frac{|R_{\text{state A to state B}}|}{\sum_{i\in S(\text{state A})}|R_i|}\mathrm{RC}_{\text{state A}} + \frac{|R_{\text{states A to state B}}|}{\sum_{j\in S(\text{state B})}|R_j|}\mathrm{RC}_{\text{state B}}, \tag{6}$$

$$\mathrm{RC}_{\text{harvest of state A}} = \frac{|R_{\text{harvest of state A}}|}{\sum_{i\in S(\text{state A})}|R_i|}\mathrm{RC}_{\text{state A}}, \tag{7}$$

Here Y_i denotes the transition or harvest. $\mathrm{RC}_{\text{state}}$ denotes the state-level relative contribution. $\mathrm{RC}_{\text{state A to state B}}$ denotes the estimated relative contribution of that transition to the variability of LULCC-induced NSWS, and $\mathrm{RC}_{\text{harvest of state A}}$ denotes the estimated relative contribution for the harvest of that state (if present). The index sets S (state A) and S (state B) collect the variables relevant to each state, namely all incoming and outgoing transitions involving that state and, for states with harvest, the harvest term. Table 4 provides details for the variables included for each state. Thus, the relative contributions sum to 1 for both individual grid cells and the area mean.

The sign of the association between a given transition or harvest and LULCC-induced NSWS is determined by the sign of the ridge regression coefficient (positive indicates a positive correlation). However, this sign information is lost when computing the relative contribution in Eq. (6). As such, we also apply a sign-preserving formulation of the relative contribution, defined following Eq. (8):

$$\mathrm{RC}_{\text{state A to state B}} = \frac{R_{\text{states A to state B}}}{\sum_{i\in S(\text{state A})}|R_i|}\mathrm{RC}_{\text{state A}} + \frac{R_{\text{states A to state B}}}{\sum_{j\in S(\text{state B})}|R_j|}\mathrm{RC}_{\text{state B}}, \tag{8}$$

This method does not enforce that relative contributions sum to 1 and is used solely to display the correlation sign. The resulting relative contributions may differ slightly from those of the previous method, yet their magnitudes still indicate how strongly a given transition or harvest contributes to LULCC-induced NSWS variability at a given location.

2.7 Model evaluation

The performance of each model on NSWS simulation was evaluated over 1970–2014 using correlation coefficients, modeled-to-observed trend ratios, root-mean-square error (RMSE), and the skill score (Shen et al., 2021; Shen et al., 2022a; Yuan et al., 2025). All metrics were computed from the spatially averaged NSWS time series over China, with the Tibetan Plateau masked out. The sparse and uneven station coverage there makes the gridded CN05.1 NSWS unreliable (Minola et al., 2024), while coarse-resolution models poorly resolve its complex terrain. The skill score is calculated using

Table 4. Variables relevant to each land state.

State	
Cropland	Cropland to Grazing; Cropland to Secondary; Cropland to Urban; Grazing to Cropland; Primary to Cropland; Secondary to Cropland; Urban to Cropland
Grazing	Grazing to Cropland; Grazing to Secondary; Grazing to Urban; Cropland to Grazing; Primary to Grazing; Secondary to Grazing; Urban to Grazing
Primary	Primary to Cropland; Primary to Grazing; Primary to Secondary; Primary to Urban; Primary harvest
Secondary	Secondary to Cropland; Secondary to Grazing; Secondary to Urban; Secondary harvest; Cropland to Secondary; Grazing to Secondary; Primary to Secondary; Urban to Secondary
Urban	Urban to Cropland; Urban to Grazing; Urban to Secondary; Cropland to Urban; Grazing to Urban; Primary to Urban; Secondary to Urban

the following equation:

$$\text{Skill score} = \frac{(1+\text{CC})^2}{(\text{SDR}+\frac{1}{\text{SDR}})^2}, \quad (9)$$

where CC refers to the correlation coefficient, and SDR refers to the standard deviation ratio between the observations and simulations.

3 Results

3.1 LULCC-induced NSWS changes

We first examine the performance of individual models and the conventional multi-model ensemble (MME), defined here as the equal-weight arithmetic mean of the nine models (with the ensemble members of each model averaged first), in simulating observed NSWS over China. Figure 1a–d show that the original outputs of LUMIP models struggle to simulate observed NSWS over China, even for spatially averaged time series. Correlation coefficients between observations and models are generally below 0.5 and even fail to reach statistical significance, except for UKESM1-0-LL (Fig. 1a). Across models, NSWS trends are substantially underestimated, with simulated trends generally being one tenth of the observed trend or less (Fig. 1b). RMSEs are comparable across models at about 0.25 m s^{-1} (roughly 10 % of the observed mean of 2.56 m s^{-1}), suggesting the mean state is reasonably captured (Fig. 1c). Meanwhile, skill scores for both individual models and the MME are generally below 0.1, indicating limited skill (Fig. 1d). In general, individual models perform poorly in terms of correlation, trend magnitude, and the overall skill score, whereas mean NSWS is reproduced well. Moreover, the MME offers no clear advantage over the individual models.

Although individual models generally perform poorly, their results differ, and some perform better in specific aspects, possibly owing to a more realistic treatment of factors affecting NSWS, such as LULCC. Among individual models, UKESM1-0-LL performs best, exhibiting a statistically significant correlation coefficient and trend while attaining the smallest RMSE. To gain more insight into the ability of models to simulate NSWS trends, we further compare the spatial distribution of NSWS trends over China among observations, the MME, and UKESM1-0-LL. Observations show a widespread decline in NSWS across China (Fig. 1e). However, neither the MME nor UKESM1-0-LL reproduces this broad weakening, especially over northern China, and their trend magnitudes are much smaller than those in observations (Fig. 1f and g). Notably, the MME shows significant increasing trends in some regions, which is a problem much less evident in UKESM1-0-LL. This indicates that the MME provides limited improvement over the individual models (Fig. 1f). This limitation may stem from the generally weak skill of the constituent models. Equal-weight averaging likely dilutes the signal and propagates inaccuracies, offsetting potential gains (Fig. 1a–d).

In contrast, by assigning greater weight to models with higher skill, ridge regression can help mitigate the limitations of equal-weight averaging. The ridge regression model performs better across all nationally averaged NSWS metrics and spatial trend patterns for 1970–2014, outperforming both individual models and the multi-model ensemble. The pattern correlation coefficient is 0.86 ($p < 0.01$). Although ridge regression still underestimates the mean trend (the trend ratio is around 0.4, meaning roughly 40 % of the observed trend), its improvement over individual models and the equal-weight ensemble is substantial, with the RMSE being less than 0.20 m s^{-1}. Considering correlation together with the standard deviation ratio, the composite skill score is higher (around 0.4). For spatial patterns, ridge regression shows clear improvement, avoiding artificial increases over South China and yielding trend magnitudes closer to observations (Fig. 1h). Overall, ridge regression provides consistent gains in both the national-mean metrics and the spatial pattern, offering a more reliable reconstruction of the observed NSWS than either individual models or the MME. Because the LULCC-induced signal is obtained as the dif-

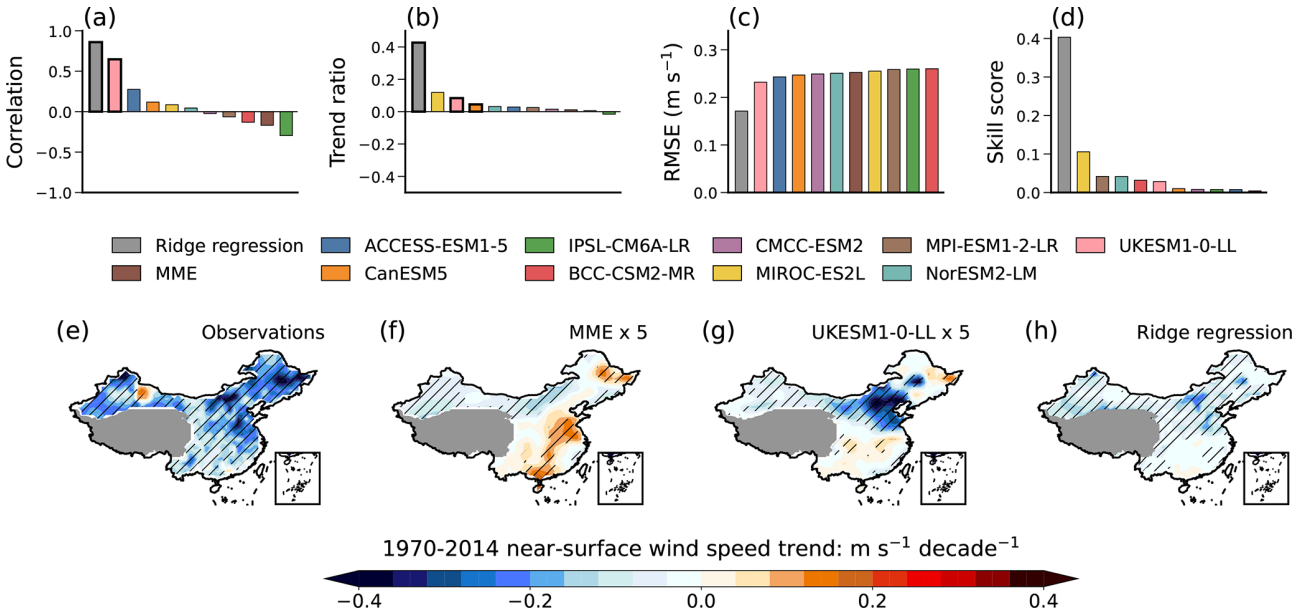


Figure 1. Evaluation of the ability of LUMIP models in simulating NSWS and spatial distribution of NSWS trends (m s^{-1} per decade) over China during 1970–2014. **(a)–(d)** report the correlation coefficient, the modeled-to-observed trend ratio relative to the CN05.1 observational dataset, the RMSE, and the skill score for spatially averaged NSWS time series over China (with Tibetan Plateau masked). Black bold bars indicate correlations statistically significant at the 0.01 level in **(a)** and trends statistically significant at the 0.01 level in **(b)**. **(e–h)** show the spatial distributions of NSWS trends from observations, MME, UKESM1-0-LL, and ridge regression, respectively. Hatching indicates a statistically significant trend at the 0.01 level. The MME and UKESM1-0-LL trends are relatively small; for comparability, panels **(f)** and **(g)** show trends scaled by five times.

ference between calibrated simulations (Sect. 2.4), this improved skill is a prerequisite for the attribution that follows.

Given the superior performance of ridge regression relative to the MME and any single model, we employ it to derive the historical LULCC-induced NSWS signals. Using coefficients derived by regressing historical simulations on observations, we bias-correct hist-noLu and compute the historical minus hist-noLu-difference (Sect. 2.4). Figure 2 shows the LULCC-induced NSWS changes derived from ridge regression, alongside results from the MME and UKESM1-0-LL. According to ridge regression, the averaged NSWS time series over China (excluding the Tibetan Plateau) exhibits no significant trend (Fig. 2a). The corresponding spatial pattern of NSWS trends shows a statistically significant increase in southern China, whereas the decrease in northern China is not significant (Fig. 2b). The ridge regression model estimate agrees more closely with UKESM1-0-LL than with the MME, suggesting that the correction relies more on models whose behavior better matches observations (Fig. 2b–d). Compared with the ridge regression, both the MME and UKESM1-0-LL exhibit implausible, widespread LULCC-induced increases in NSWS (Fig. 2b–d). These responses may partly reflect their limited ability to reproduce historical NSWS changes, as most models simulate widespread increases, in stark contrast to the pronounced nationwide decline observed across China.

3.2 Relative contributions of LULCC types

We further attribute LULCC-induced NSWS to individual LULCC types. Our premise is that, with other forcings held constant, different land states and management practices correspond to different expected NSWS, so that changes in land-state composition and management lead to NSWS changes (Sect. 2.6). Figure 3 shows the relative contributions of individual land states and management practices to NSWS variability in China during 1970–2014. In the attribution based on land-state and land-management variables, contributions from different states and management practices are comparable in magnitude, indicating that NSWS changes arise from various factors (Fig. 3a). Among them, grazing contributes the most, followed by secondary land. Comparatively, the variability associated with urban change is the smallest among the five land states and two management practices, likely because LUH2 shows very limited urban extent at the national scale, as the national mean urban fraction was only around 0.5 % during 1970–2014, whereas grazing covers about 28 % and secondary vegetation about 21 %. Many regions in China contain no urban land at all. Hence, it is reasonable that urban contributes the least to variability.

Changes in a LULCC state do not occur in isolation. In general, they arise from land transitions involving at least one other state. The results from the first step quantify the importance of each state for NSWS on its own, whereas the

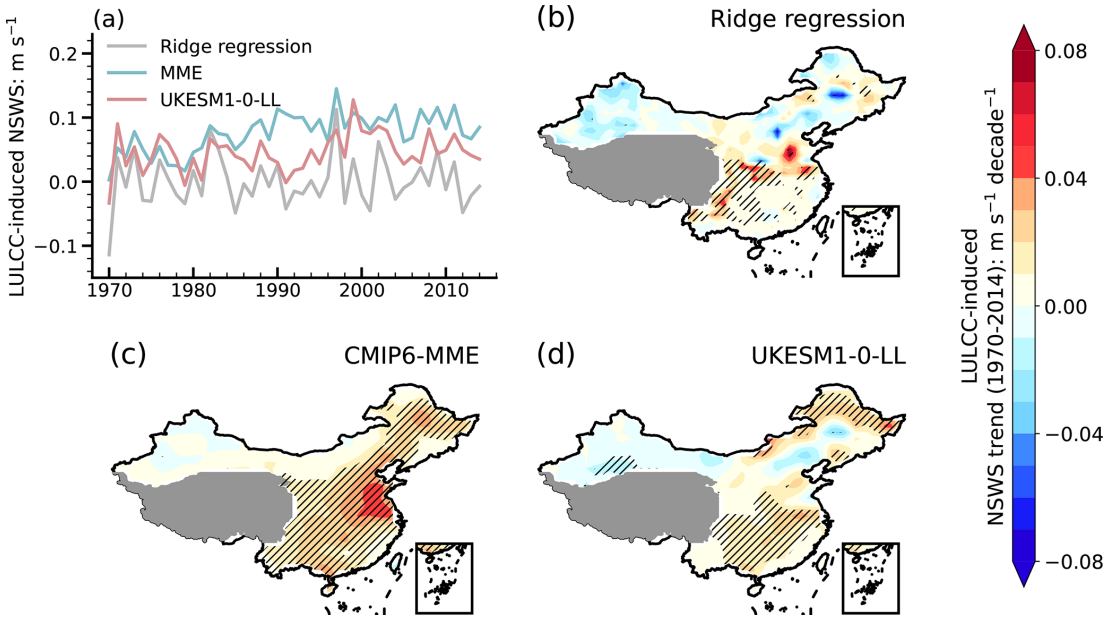


Figure 2. Averaged annual-mean and spatial trend patterns of LULCC-induced NSWS over China during 1970–2014. **(a)** Averaged annual-mean time series of LULCC-induced NSWS over China during 1970–2014 for ridge regression, MME and UKESM1-0-LL. Spatial trend patterns of LULCC-induced NSWS over China during 1970–2014 for **(b)** ridge regression, **(c)** MME and **(d)** UKESM1-0-LL. Hatching indicates a statistically significant trend at the 0.01 level.

results from the second step identify which transitions contribute most to NSWS changes and focus the analysis on land change processes, which better aligns with intuition. Furthermore, we decompose the contribution of each state into specific transitions. The expansion of grazing land (mainly from primary land and secondary land) makes a substantial contribution to LULCC-induced NSWS variability, accounting for 28.93 % among all transition types. Among urban land changes, only the crop-to-urban transition ranks among the top ten contributors, indicating that rapid, cropland-consuming urbanization does affect NSWS (Fig. 3b). However, due to its small spatial footprint, urbanization remains a modest contributor to the national average.

Figure 3 also illustrates that the same land-use transition or management practice can lead to distinct NSWS responses across regions, supporting the complex nature of LULCC impacts in China. Overall, the transition from primary land to grazing land emerges as the dominant contributor to LULCC-induced increases in NSWS, and ridge regression attribution for 1970–2014 further confirms this, as positive contributions are more widespread (Fig. 3c). This transition happens mainly in Inner Mongolia, northern China, where intensive livestock production and the arid to semi-arid climate favor pasture expansion (Fig. 3e). Mechanistically, relative to grazing land, primary land might support more diverse and structurally complex vegetation, yielding greater surface roughness; replacing it with grazing land reduces roughness and can enhance NSWS. Consequently, the decline in primary land together with the expansion of grazing land, which might reflect growth of the livestock sector, likely contributed to the observed rise in NSWS over China in recent decades.

Following the primary-to-grazing transition, fertilization acts as the second largest positive driver of LULCC-induced NSWS changes (Fig. 3b). Between the two examined management practices, fertilization exerts a substantially stronger impact than irrigation, as fertilization explains $\sim 16\,\%$ of LULCC-induced NSWS variability, compared with $\sim 10\,\%$ for irrigation. Mechanistically, fertilization stimulates vegetation growth and canopy closure, which would be expected to increase aerodynamic roughness and perturb near-surface flow. Concomitant increases in vegetation cover may also modify surface albedo and evapotranspiration, thereby affecting boundary-layer stability and local winds. Accordingly, fertilization may exert dual effects on NSWS through aerodynamic and thermodynamic processes. In our results, increases in fertilization are associated with NSWS enhancement across much of China, except in northwestern China. This suggests that the positive effect, on balance, is more common (Fig. 3d and f).

3.3 Projected LULCC-induced NSWS

Understanding the projected responses of NSWS to future LULCC is crucial for long-term wind-energy planning and climate mitigation. We first examine the future NSWS trends under SSP1-2.6 and SSP3-7.0 to provide the background for interpreting the LULCC-induced changes (Fig. S1 in the

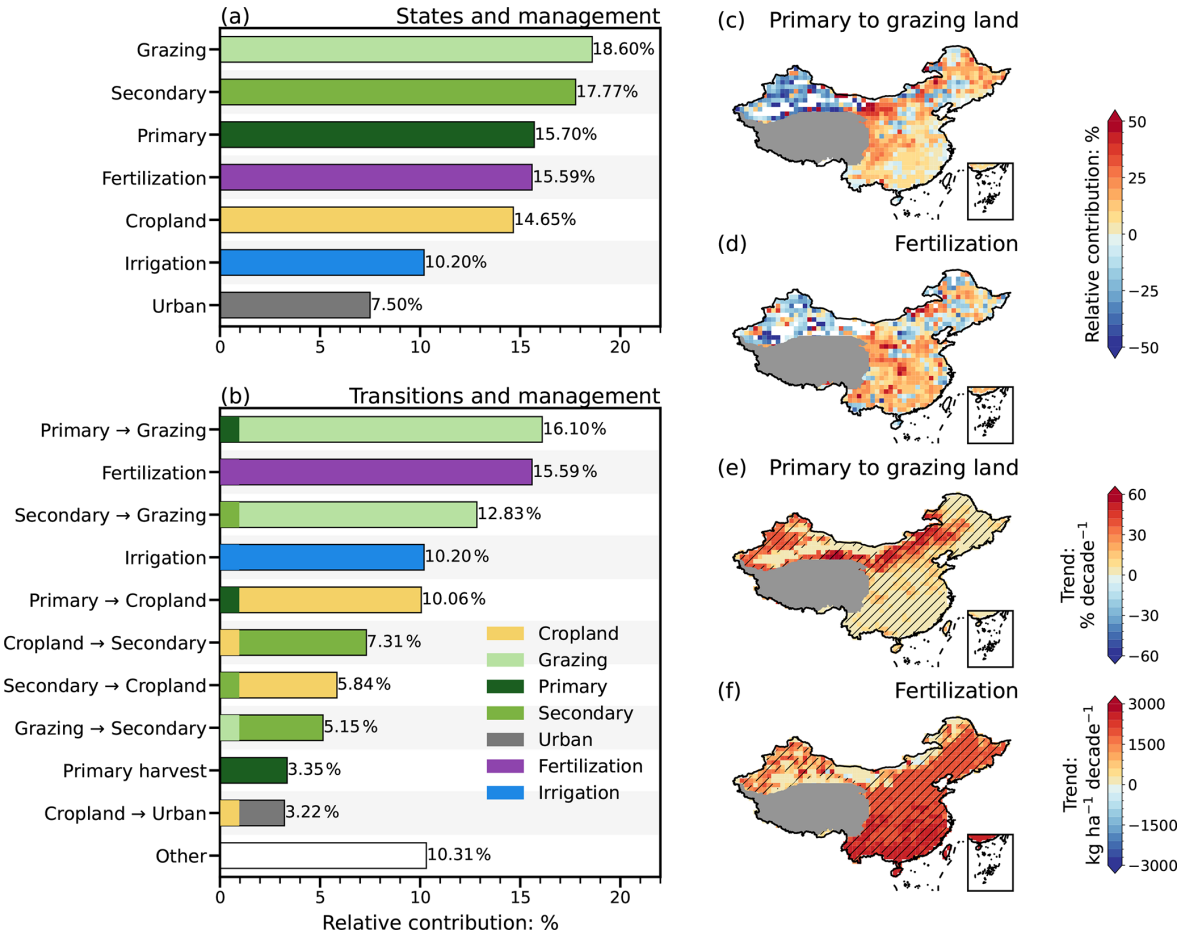


Figure 3. Relative contributions of LULCC types to LULCC-induced NSWS changes over China, and the spatial patterns and trends of contributions from the primary-to-grazing transition and fertilization. **(a)** Contributions by land states and management. **(b)** Contributions by transitions and management. The relative contribution of states was estimated using ridge regression between LULCC-induced changes and state and management variables; the transition contribution was then derived from these state-based contributions. In each horizontal bar except harvest, the left segment indicates the origin land states, and the right segment indicates the destination land states. Only the top ten transitions or harvest categories with the largest relative contributions are shown. **(c, d)** Spatial patterns of the relative contributions of the **(c)** primary-to-grazing transition and **(d)** fertilization. **(e, f)** Spatial patterns of the trends of the **(e)** primary-to-grazing transition and **(f)** fertilization. Hatching indicates a statistically significant trend at the 0.01 level.

Supplement). Overall, the continued decline in NSWS is largely maintained under SSP3-7.0, with stronger decreases over northern China, broadly consistent with the spatial pattern of the historical simulated trend. In contrast, under SSP1-2.6, the decline weakens and NSWS begins to recover in some regions. Within each scenario, the near- and long-term patterns are broadly similar, while the mid-term shows some spatial differences. Against this background, we apply the ridge regression model calibrated on the historical experiments to the LUMIP future experiments (Sect. 2.4) to estimate LULCC-induced NSWS changes under a low-emission (SSP1-2.6) and a high-emission (SSP3-7.0) background. Because the land-use forcing is swapped between the two scenarios, the difference between each swap experiment and its parent scenario isolates the effect of the land-use trajectory from that of the greenhouse gas (GHG) forcing.

Comparing the swap experiments with their parent scenarios tests whether LULCC trajectories alone could dominate future NSWS changes. As illustrated in Fig. 4, the difference between ssp126-ssp370Lu and ssp126 is substantially larger than that between ssp370 and ssp370-ssp126Lu. This pattern suggests that the potential effects of minimal-regulation land-use trajectories on NSWS under low emission scenarios are more pronounced than those of sustainable land-use trajectories under high emission scenarios. Under SSP1-2.6, minimal-regulation trajectories are projected to amplify regional NSWS increases, especially in western China (Fig. 4a–c). In this setting, relatively low GHG forcing likely heightens the sensitivity of NSWS to land manage-

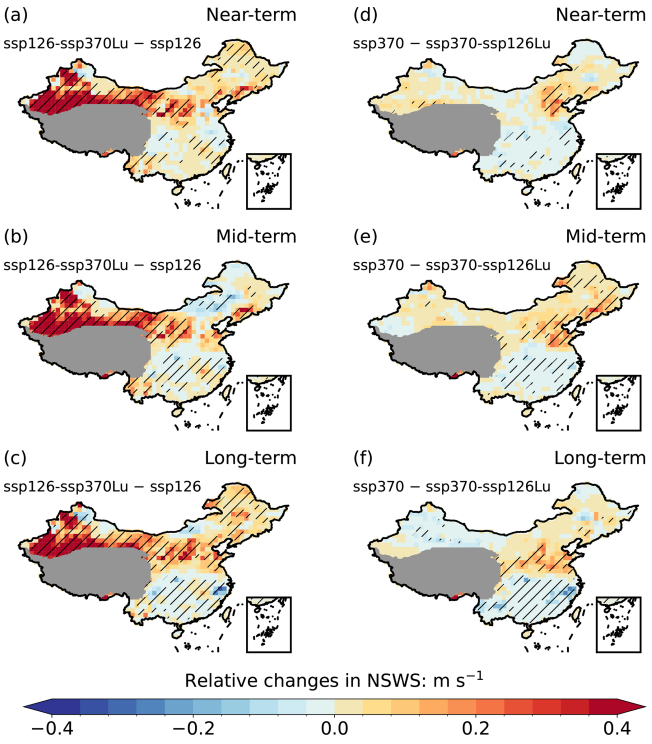


Figure 4. Future LULCC-induced NSWS changes. **(a–c)** Differences in climatological NSWS between ssp126-ssp370Lu and ssp126 for **(a)** the near term (2020–2040), **(b)** the mid term (2040–2060), and **(c)** the long term (2080–2099); **(d)–(f)** as in **(a)–(c)**, but for ssp370 minus ssp370-ssp126Lu. Hatching indicates grid cells where the differences between the paired experiments are statistically significant at the 0.01 level based on a Student's t-test across years. ssp126, ssp370, ssp126-ssp370Lu, and ssp370-ssp126Lu denote different experimental designs.

ment, underscoring the necessity for well-designed, sustainable land-use policies to mitigate climate impacts (Lawrence et al., 2016). Under SSP3-7.0, the overall LULCC-induced signal is small (Fig. 4d–f). A plausible explanation is that the dominant influence of high GHG emissions overwhelms LULCC effects, with atmospheric changes caused by warming largely governing NSWS. Together, these results emphasize the need to integrate land-use policy with emissions-mitigation strategies to optimize wind resource availability and strengthen ecosystem resilience in a changing climate. Moreover, the differences between periods are modest, which might indicate that the LULCC impact is approximately constant under the same forcing.

4 Discussion and conclusions

Our study provides a comprehensive evaluation of LULCC-driven NSWS changes across China during 1970–2014, revealing an overall positive contribution from LULCC. This overarching positive effect contrasts sharply with prevailing assumptions in the NSWS community, which have traditionally linked LULCC primarily to widespread wind stilling. Meanwhile, unlike previous studies, we find that urbanization is not a dominant driver of NSWS changes, with its overall contribution substantially outweighed by the two most influential positive drivers, the primary-to-grazing transition and widespread fertilizer use. Furthermore, in future scenarios, the potential influence of LULCC on NSWS is substantially more pronounced under low-emission backgrounds than under high-emission extremes. Accurately capturing its net climatic impact fundamentally requires disentangling the distinct, and sometimes opposing, roles of specific land-use transitions and management practices.

Differences in how CMIP6 models parameterize land-surface processes fundamentally drive the inter-model spread identified in this study. The mathematical and physical treatment of LULCC alters vegetation properties, surface roughness, soil moisture, and surface energy partitioning, thereby influencing sensible heating, boundary-layer development, and ultimately near-surface momentum. In this context, the superior performance of specific models, such as UKESM1-0-LL, may stem from a more realistic and interactive representation of land-atmosphere coupling, such as dynamic vegetation responses and intricate canopy radiation schemes. This mechanistic advantage elucidates the efficacy of our ridge regression approach, which appropriately assigns greater statistical weight to models exhibiting higher physical skill. Nevertheless, although our LUMIP-based framework provides a perspective on the relative contributions of individual LULCC types, the absolute magnitudes of these estimates carry uncertainties tied to the base parameterizations in models. A related caveat is that the ridge-regression reconstruction still underestimates the observed national-mean NSWS trend (trend ratio of about 0.4; Fig. 1b). Part of the discrepancy between the reconstructed and observed trends likely reflects internal variability that free-running simulations cannot be expected to reproduce in phase with the observations (Shen et al., 2025). Because the LULCC-induced signal is derived as the difference between two experiments calibrated with the same weights (Eq. 1), and the relative contributions in Sect. 3.2 are calculated as ratios (Eqs. 4, 6 and 7), we expect this underestimation to primarily affect the absolute magnitude of the LULCC contributions, while their sign, spatial pattern, and relative ranking are likely to be less affected. Nevertheless, the absolute magnitudes of the LULCC-induced changes, including the projected changes in Sect. 3.3, should be interpreted with this additional uncertainty in mind.

Whereas previous studies argued that LULCC contributed uniformly to the historical decline of NSWS over China, our results indicate spatially heterogeneous contributions; even at the national scale, the LULCC-induced NSWS trend is statistically neutral. Furthermore, whereas prior observation-based attributions emphasized the role of urbanization in NSWS changes (Li et al., 2018; Zhang and Wang, 2021), we

find urbanization's overarching contribution to be relatively minor, aligning well with its extremely limited areal fraction nationwide. These discrepancies are directly attributable to methodological differences. Conventional observation-minus-reanalysis approaches treat LULCC as an aggregated residual and would suffer from spatial biases due to the over-representation of urban meteorological stations. By utilizing controlled LUMIP experiments, our study circumvents this urban bias and demonstrates that extensive landscape transformations, rather than localized urban expansion, dictate the overall NSWS response.

The mechanisms by which individual LULCC types affect NSWS remain largely unresolved. For example, our results indicate that increases in fertilization have contributed positively to NSWS across much of China, with the strongest signals in the east. Fertilization can affect NSWS through competing processes. Enhanced vegetation growth increases aerodynamic roughness and surface drag, which would tend to reduce NSWS. At the same time, fertilization-induced changes in vegetation state, evapotranspiration and surface energy partitioning can modify boundary-layer stability, turbulent mixing and local thermal circulations. The predominantly positive NSWS response over much of China therefore suggests that, in the simulations, these thermodynamic and dynamical adjustments offset, and in many regions exceed, the direct wind-reducing effect of increased surface drag. The NSWS response to fertilization should thus be interpreted as the net outcome of these competing land–atmosphere processes rather than as a direct roughness effect. By contrast, irrigation appears to exert a more uniform, thermodynamically mediated influence as it cools the land surface, stabilizes soil moisture and the boundary layer, and reduces wind erosion in arid regions (Yu and Leng, 2022). These inferred mechanisms necessitate future validation using high-resolution regional climate models coupled with explicit crop-management modules.

Future work should further examine how LULCC interacts with other atmospheric variables, how its effects on NSWS vary across climatic regions, and how land-use transitions are shaped by broader socio-economic drivers. Ultimately, integrating granular land-use and land-management policies with broader GHG mitigation strategies will be indispensable for optimizing future wind-energy resources and ensuring regional climate resilience.

Code availability. The analysis was conducted using Python, and the code used to support the findings of this study is available from the corresponding author upon reasonable request.

Data availability. All data used in this study are publicly available. The CMIP6 and LUMIP model outputs used in this study are publicly available through the Earth System Grid Federation (ESGF; https://wcrp-cmip.org/cmip-data-access/; last access: 19 February 2026). The CN05.1 observational dataset is available from Wu and Gao (2013). The Land-Use Harmonization version 2 (LUH2) historical dataset is available from the LUH2 project website (https://luh.umd.edu; last access: 19 February 2026).

Supplement. The supplement related to this article is available online at https://doi.org/10.5194/esd-17-1765-2026-supplement.

Author contributions. All authors reviewed and revised the manuscript. CS and YC designed the study. HSY conducted the visualization and analysis together with CS.

Competing interests. The contact author has declared that none of the authors has any competing interests.

Disclaimer. Publisher's note: Copernicus Publications remains neutral with regard to jurisdictional claims made in the text, published maps, institutional affiliations, or any other geographical representation in this paper. The authors bear the ultimate responsibility for providing appropriate place names. Views expressed in the text are those of the authors and do not necessarily reflect the views of the publisher.

Acknowledgements. We acknowledge the open-source community for the quiet efficiency behind our analysis.

Financial support. This work is supported by the Stiftelsen Längmanska kulturfonden (grant no. BA24-0484), Svenska Forskningsrådet Formas (grant no. 2023-01648), Stiftelsen Åforsk (grant no. 24-707), Herbert & Karin Jacobssons Stiftelse (grant no. 2025-465), Juan de la Cierva Fellowship (grant no. JDC2025-056820-I), and Adlerbertska Forskningsstiftelsen (grant no. AF2024-0069). Zi-Han Wang is supported by the Innovation and Entrepreneurship Training Program for College Students of Yunnan University (grant no. S202307019).

Review statement. This paper was edited by Daniel Kirk-Davidoff and reviewed by two anonymous referees.

References

Andres-Martin, M., Azorin-Molina, C., Shen, C., Fernández-Alvarez, J. C., Gimeno, L., Vicente-Serrano, S. M., and Zha, J.: Uncertainty in surface wind speed projections over the Iberian Peninsula: CMIP6 GCMs versus a WRF-RCM, Ann. N. Y. Acad. Sci., 1529, 101–108, https://doi.org/10.1111/nyas.15063, 2023.

Bring, J.: How to Standardize Regression Coefficients, Am. Stat., 48, 209–213, https://doi.org/10.1080/00031305.1994.10476059, 1994.

Chini, L., Hurtt, G., Sahajpal, R., Frolking, S., Klein Goldewijk, K., Sitch, S., Ganzenmüller, R., Ma, L., Ott, L., Pongratz, J., and Poulter, B.: Land-use harmonization datasets for annual global carbon budgets, Earth Syst. Sci. Data, 13, 4175–4189, https://doi.org/10.5194/essd-13-4175-2021, 2021.

Christidis, N., Stott, P. A., Hegerl, G. C., and Betts, R. A.: The role of land use change in the recent warming of daily extreme temperatures, Geophys. Res. Lett., 40, 589–594, https://doi.org/10.1002/grl.50159, 2013.

Chuan, T., Wu, J., Zha, J. L., Zhao, D. M., Shen, C., Fan, W. X., and Jiang, H. P.: Asynchronous changes in terrestrial near-surface wind speed among regions across China from 1973 to 2017, Atmos. Res., 300, 107220, https://doi.org/10.1016/j.atmosres.2024.107220, 2024.

Dunn, R. J. H., Azorin-Molina, C., Menne, M. J., Zeng, Z. Z., Casey, N. W., and Shen, C.: Reduction in reversal of global stilling arising from correction to encoding of calm periods, Environ. Res. Commun., 4, 061003, https://doi.org/10.1088/2515-7620/ac770a, 2022.

Grömping, U.: Relative Importance for Linear Regression in R: The Package relaimpo, J. Stat. Softw., 17, 1–27, https://doi.org/10.18637/jss.v017.i01, 2006.

Hoerl, A. E. and Kennard, R. W.: Ridge Regression: Biased Estimation for Nonorthogonal Problems, Technometrics, 12, 55–67, https://doi.org/10.1080/00401706.1970.10488634, 1970.

Hurtt, G. C., Chini, L., Sahajpal, R., Frolking, S., Bodirsky, B. L., Calvin, K., Doelman, J. C., Fisk, J., Fujimori, S., Klein Goldewijk, K., Hasegawa, T., Havlik, P., Heinimann, A., Humpenöder, F., Jungclaus, J., Kaplan, J. O., Kennedy, J., Krisztin, T., Lawrence, D., Lawrence, P., Ma, L., Mertz, O., Pongratz, J., Popp, A., Poulter, B., Riahi, K., Shevliakova, E., Stehfest, E., Thornton, P., Tubiello, F. N., van Vuuren, D. P., and Zhang, X.: Harmonization of global land use change and management for the period 850–2100 (LUH2) for CMIP6, Geosci. Model Dev., 13, 5425–5464, https://doi.org/10.5194/gmd-13-5425-2020, 2020.

Ito, A. and Hajima, T.: Biogeophysical and biogeochemical impacts of land-use change simulated by MIROC-ES2L, Prog. Earth Planet. Sci., 7, 54, https://doi.org/10.1186/s40645-020-00372-w, 2020.

Lawrence, D. M., Hurtt, G. C., Arneth, A., Brovkin, V., Calvin, K. V., Jones, A. D., Jones, C. D., Lawrence, P. J., de Noblet-Ducoudré, N., Pongratz, J., Seneviratne, S. I., and Shevliakova, E.: The Land Use Model Intercomparison Project (LUMIP) contribution to CMIP6: rationale and experimental design, Geosci. Model Dev., 9, 2973–2998, https://doi.org/10.5194/gmd-9-2973-2016, 2016.

Li, Y., Wang, Y., Chu, H. Y., and Tang, J. P.: The climate influence of anthropogenic land-use changes on near-surface wind energy potential in China, Chin. Sci. Bull., 53, 2859–2866, https://doi.org/10.1007/s11434-008-0360-z, 2008.

Li, Z. B., Xu, Y., Yuan, H. S., Chang, Y. L., and Shen, C.: AMO footprint of the recent near-surface wind speed change over China, Environ. Res. Lett., 19, 114031, https://doi.org/10.1088/1748-9326/ad7ee4, 2024.

Li, Z.-B., Sun, M., Shen, C., and Chen, D.: ENSO-Driven Seasonal Variability in Near-Surface Wind Speed and Wind Power Potential Across China, Geophys. Res. Lett., 52, e2025GL115537, https://doi.org/10.1029/2025GL115537, 2025.

Li, Z. Q., Song, L. L., Ma, H., Xiao, J. J., Wang, K., and Chen, L.: Observed surface wind speed declining induced by urbanization in East China, Clim. Dynam., 50, 735–749, https://doi.org/10.1007/s00382-017-3637-6, 2018.

Liu, Y., Zhou, L., Qin, Y., Azorin-Molina, C., Shen, C., Xu, R., and Zeng, Z.: Impacts of anemometer changes, site relocations and processing methods on wind speed trends in China, Atmos. Meas. Tech., 17, 1123–1131, https://doi.org/10.5194/amt-17-1123-2024, 2024.

Long, Y. X., Xu, C. C., Liu, F., Liu, Y. C., and Yin, G.: Evaluation and Projection of Wind Speed in the Arid Region of Northwest China Based on CMIP6, Remote Sens., 13, 4076, https://doi.org/10.3390/rs13204076, 2021.

Minola, L., Lönn, J., Azorin-Molina, C., Zhou, C. L., Engström, E., Wern, L., Hellström, S., Zhang, G. F., Shen, C., Pezzoli, A., and Chen, D. L.: The contribution of large-scale atmospheric circulation to variations of observed near-surface wind speed across Sweden since 1926, Climatic Change, 176, 54, https://doi.org/10.1007/s10584-023-03525-0, 2023.

Minola, L., Zhang, G. F., Ou, T. H., Kukulies, J., Curio, J., Guijarro, J. A., Deng, K. Q., Azorin-Molina, C., Shen, C., Pezzoli, A., and Chen, D. L.: Climatology of near-surface wind speed from observational, reanalysis and high-resolution regional climate model data over the Tibetan Plateau, Clim. Dynam., 62, 933–953, https://doi.org/10.1007/s00382-023-06931-3, 2024.

O'Neill, B. C., Tebaldi, C., van Vuuren, D. P., Eyring, V., Friedlingstein, P., Hurtt, G., Knutti, R., Kriegler, E., Lamarque, J.-F., Lowe, J., Meehl, G. A., Moss, R., Riahi, K., and Sanderson, B. M.: The Scenario Model Intercomparison Project (ScenarioMIP) for CMIP6, Geosci. Model Dev., 9, 3461–3482, https://doi.org/10.5194/gmd-9-3461-2016, 2016.

Popp, A., Calvin, K., Fujimori, S., Havlik, P., Humpenöder, F., Stehfest, E., Bodirsky, B. L., Dietrich, J. P., Doelmann, J. C., Gusti, M., Hasegawa, T., Kyle, P., Obersteiner, M., Tabeau, A., Takahashi, K., Valin, H., Waldhoff, S., Weindl, I., Wise, M., Kriegler, E., Lotze-Campen, H., Fricko, O., Riahi, K., and van Vuuren, D. P.: Land-use futures in the shared socioeconomic pathways, Glob. Environ. Change, 42, 331–345, https://doi.org/10.1016/j.gloenvcha.2016.10.002, 2017.

Pryor, S. C. and Barthelmie, R. J.: A global assessment of extreme wind speeds for wind energy applications, Nat. Energy, 6, 268–276, https://doi.org/10.1038/s41560-020-00773-7, 2021.

Santos, J. F., Schickhoff, U., ul Hasson, S., and Böhner, J.: Biogeophysical Effects of Land-Use and Land-Cover Changes in South Asia: An Analysis of CMIP6 Models, Land, 12, 880, https://doi.org/10.3390/land12040880, 2023.

Shen, C., Zha, J., Wu, J., and Zhao, D. M.: Centennial-Scale Variability of Terrestrial Near-Surface Wind Speed over China from Reanalysis, J. Climate, 34, 5829–5846, https://doi.org/10.1175/Jcli-D-20-0436.1, 2021.

Shen, C., Zha, J., Li, Z., Azorin-Molina, C., Deng, K., Minola, L., and Chen, D.: Evaluation of global terrestrial near-surface wind speed simulated by CMIP6 models and their future projections, Ann. N. Y. Acad. Sci., 1518, 249–263, https://doi.org/10.1111/nyas.14910, 2022a.

Shen, C., Zha, J., Wu, J., Zhao, D., Azorin-Molina, C., Fan, W., and Yu, Y.: Does CRA-40 outperform other reanalysis products in evaluating near-surface wind

speed changes over China?, Atmos. Res., 266, 105948, https://doi.org/10.1016/j.atmosres.2021.105948, 2022b.

Shen, C., Yuan, H. S., Li, Z. B., Yang, X. Y., Minola, L., Chang, Y. L., and Chen, D. L.: March Near-Surface Wind Speed Hiatus Over China Since 2011, Geophys. Res. Lett., 50, e2023GL104230, https://doi.org/10.1029/2023GL104230, 2023.

Shen, C., Li, Z. B., Yuan, H. S., Yu, Y., Lei, Y. D., and Chen, D. L.: Increases of Offshore Wind Potential in a Warming World, Geophys. Res. Lett., 51, e2024GL109494, https://doi.org/10.1029/2024GL109494, 2024.

Shen, C., Yuan, H.-S., Li, Z.-B., Piao, J., Chang, Y., and Chen, D.: Unravelling the future role of internal variability in South Asian near-surface wind speed, Earth Syst. Dynam., 16, 1959–1969, https://doi.org/10.5194/esd-16-1959-2025, 2025.

Shen, C., Sun, Z. D., Xu, Y., Yuan, H. S., and Chang, Y.: Divergent Forest Cover Changes Dominate Inter-Model Spread in Near-Surface Wind Speed Trends Over China, Geophys. Res. Lett., 53, e2026GL124057, https://doi.org/10.1029/2026gl124057, 2026.

Sierra, J. P., Junquas, C., Espinoza, J. C., Segura, H., Condom, T., Andrade, M., Molina-Carpio, J., Ticona, L., Mardoñez, V., Blacutt, L., Polcher, J., Rabatel, A., and Sicart, J. E.: Deforestation impacts on Amazon-Andes hydroclimatic connectivity, Clim. Dynam., 58, 2609–2636, https://doi.org/10.1007/s00382-021-06025-y, 2022.

Tang, T., Lee, X., Zhang, K., Cai, L., Lawrence, D. M., and Shevliakova, E.: Biophysical Impact of Land-Use and Land-Cover Change on Subgrid Temperature in CMIP6 Models, J. Hydrometeorol., 24, 373–388, https://doi.org/10.1175/Jhm-D-22-0073.1, 2023.

Tebaldi, C. and Knutti, R.: The use of the multi-model ensemble in probabilistic climate projections, Philos. T. R. Soc. A, 365, 2053–2075, https://doi.org/10.1098/rsta.2007.2076, 2007.

Tran, D. X., Pla, F., Latorre-Carmona, P., Myint, S. W., Gaetano, M., and Kieu, H. V.: Characterizing the relationship between land use land cover change and land surface temperature, ISPRS J. Photogramm., 124, 119–132, https://doi.org/10.1016/j.isprsjprs.2017.01.001, 2017.

Vautard, R., Cattiaux, J., Yiou, P., Thépaut, J. N., and Ciais, P.: Northern Hemisphere atmospheric stilling partly attributed to an increase in surface roughness, Nat. Geosci., 3, 756–761, https://doi.org/10.1038/Ngeo979, 2010.

Wang, J., Feng, J. M., Yan, Z. W., Qiu, Y., and Cao, L. J.: An analysis of the urbanization contribution to observed terrestrial stilling in the Beijing-Tianjin-Hebei region of China, Environ. Res. Lett., 15, 034062, https://doi.org/10.1088/1748-9326/ab7396, 2020.

Wang, J. M., Yang, K., Yuan, L., Liu, J. R., Peng, Z., Ren, Z. H., and Zhou, X.: Deducing Aerodynamic Roughness Length From Abundant Anemometer Tower Data to Inform Wind Resource Modeling, Geophys. Res. Lett., 51, e2024GL111056, https://doi.org/10.1029/2024GL111056, 2024.

Wang, J., Yang, K., Liu, J., Zhou, X., Ma, X., Tang, W., Yuan, L., and Ren, Z.: Improvement of near-surface wind speed modeling through refined aerodynamic roughness length in high-roughness surface regions: implementation and validation in the Weather Research and Forecasting (WRF) model version 4.0, Geosci. Model Dev., 18, 10077–10094, https://doi.org/10.5194/gmd-18-10077-2025, 2025.

Wu, H., Fu, C., Zhang, L., Mekonnen, Z. A., Zhu, Q., Yu, K., Ciais, P., Chen, J., Wang, D., Wu, H., and Yang, G.: Significant sensitivity of global vegetation productivity to terrestrial surface wind speed changes, Nat. Commun., 16, 9315, https://doi.org/10.1038/s41467-025-65000-x, 2025.

Wu, J. and Gao, X. J.: A gridded daily observation dataset over China region and comparison with the other datasets, Chin. J. Geophys., 56, 1102–1111, https://doi.org/10.6038/cjg20130406, 2013.

Wu, J., Gao, X. J., Giorgi, F., and Chen, D. L.: Changes of effective temperature and cold/hot days in late decades over China based on a high resolution gridded observation dataset, Int. J. Climatol., 37, 788–800, https://doi.org/10.1002/joc.5038, 2017.

Xu, Y., Yuan, H. S., Sun, Z. D., Chang, Y. L., and Shen, C.: EOF-Based Bias Correction of Near-Surface Wind Speed Over China Reveals Stronger Future Trends and Variability, Geophys. Res. Lett., 53, e2025GL120559, https://doi.org/10.1029/2025GL120559, 2026.

Yan, Y., Wu, J., Chao, Q. C., and Sun, Y.: Overestimation of the recent observed near-surface wind speed recovery in China, npj Clim. Atmos. Sci., 9, 49, https://doi.org/10.1038/s41612-026-01322-x, 2026.

Yang, Q., Li, M., Zu, Z., and Ma, Z.: Has the stilling of the surface wind speed ended in China?, Sci. China Earth Sci., 64, 1036–1049, https://doi.org/10.1007/s11430-020-9738-4, 2021.

Yu, L. F. and Leng, G. Y.: Global effects of different types of land use and land cover changes on near-surface air temperature, Agr. Forest Meteorol., 327, 109232, https://doi.org/10.1016/j.agrformet.2022.109232, 2022.

Yuan, H. S., Piao, J. L., Chang, Y. L., and Shen, C.: Simulated and projected near-surface wind speed in High-Resolution Model Intercomparison Project, Clim. Dynam., 63, 298, https://doi.org/10.1007/s00382-025-07792-8, 2025.

Zeng, Z. Z., Ziegler, A. D., Searchinger, T., Yang, L., Chen, A. P., Ju, K. L., Piao, S. L., Li, L. Z. X., Ciais, P., Chen, D. L., Liu, J. G., Azorin-Molina, C., Chappell, A., Medvigy, D., and Wood, E. F.: A reversal in global terrestrial stilling and its implications for wind energy production, Nat. Clim. Change, 9, 979–985, https://doi.org/10.1038/s41558-019-0622-6, 2019.

Zha, J., Wu, J., and Zhao, D.: Effects of land use and cover change on the near-surface wind speed over China in the last 30 years, Prog. Phys. Geogr. Earth Environ., 41, 46–67, https://doi.org/10.1177/0309133316663097, 2016.

Zha, J., Zhao, D. M., Wu, J., and Shen, C.: Terrestrial Near-Surface Wind Speed Variations in China: Research Progress and Prospects, J. Meteorol. Res., 35, 537–556, https://doi.org/10.1007/s13351-021-0143-x, 2021a.

Zha, J., Shen, C., Zhao, D. M., Wu, J., and Fan, W. X.: Slowdown and reversal of terrestrial near-surface wind speed and its future changes over eastern China, Environ. Res. Lett., 16, 034028, https://doi.org/10.1088/1748-9326/abe2cd, 2021b.

Zha, J., Shen, C., Li, Z. B., Wu, J., Zhao, D. M., Fan, W. X., Sun, M., Azorin-Molina, C., and Deng, K. Q.: Projected changes in global terrestrial near-surface wind speed in 1.5 °C–4.0 °C global warming levels, Environ. Res. Lett., 16, 114016, https://doi.org/10.1088/1748-9326/ac2fdd, 2021c.

Zha, J., Chuan, T., Wu, J., Zhao, D. M., Luo, M., Feng, J. M., Fan, W. X., Shen, C., and Jiang, H. P.: Attribution of Terrestrial Near-Surface Wind Speed Changes Across China at a Centennial Scale, Geophys. Res. Lett., 51, e2024GL108241, https://doi.org/10.1029/2024GL108241, 2024.

Zhang, Z. and Wang, K.: Quantifying and adjusting the impact of urbanization on the observed surface wind speed over China from 1985 to 2017, Fundam. Res., 1, 785–791, https://doi.org/10.1016/j.fmre.2021.09.006, 2021.

Zhang, Z., Xu, J., Zhang, Y., Zhuang, H., Li, S., Tao, F., and Zhang, Z.: Decadal changes in wind speed have offset and then aggravated the impact of warming on maize production in China since 1980, Nat. Commun., 16, 9739, https://doi.org/10.1038/s41467-025-64725-z, 2025.

Zhang, Z. T., Wang, K. C., Chen, D. L., Li, J. P., and Dickinson, R.: Increase in Surface Friction Dominates the Observed Surface Wind Speed Decline during 1973-2014 in the Northern Hemisphere Lands, J. Climate, 32, 7421–7435, https://doi.org/10.1175/Jcli-D-18-0691.1, 2019.

Zheng, C. W., Pan, J., and Li, C. Y.: Global oceanic wind speed trends, Ocean Coast. Manag., 129, 15–24, https://doi.org/10.1016/j.ocecoaman.2016.05.001, 2016.